Chapter 2

Capacity Optimization Nanotechnologies for Enhanced Energy Storage Systems

Natasha Ross and Emmanuel I. Iwuoha

Additional information is available at the end of the chapter

http://dx.doi.org/10.5772/62319

Abstract

Rechargeable lithium-ion battery (LIB) cathodes consist of transition metal oxide material, which reversibly (de)intercalates lithium at a high potential difference versus a carbon anode. Manganese oxide cathode material offers lower cost and toxicity than the normally used cobalt. However, $LiMn_2O_4$ suffers from capacity fading, Mn dissolution at high temperatures, and poor high rate capability. Its ultimate performance, however, depends on the morphology and electrochemical properties. In this work, Au alloyed with Fe, Pd, and Pt, respectively, was synthesized and used to improve the microstructure and catalytic activities by functionalizing $LiMn_2O_4$ via a coprecipitation calcination method. The pristine $LiMn_2O_4$ and modified materials were examined using a combination of spectroscopic and microscopic techniques along with in-detail galvanostatic charge–discharge tests. Microscopic results revealed that the modified composite cathode materials had high phase purity, highly crystallized particles, and more regular morphological structures with narrow size distributions. Galvanostatic charge–discharge testing indicated that the initial discharge capacities of $LiM_xMn_{2-x}O_4$ at 0.1 C for $M_{0.02}$=PtAu, FeAu, and PdAu were 147, 155.5, and 160.2 mAh g^{-1}, respectively. The enhancement of the capacity retention and higher electrode coulombic efficiency of the modified materials were significant, especially at high C rate. At enlarged cycling potential ranges, the $Li(M)_{0.02}Mn_{1.98}O_4$ samples delivered relevant discharge capacities (70, 80, and 90 mAh g^{-1}) compared to $LiMn_2O_4$ (45 mAh g^{-1}).

Keywords: Energy storage, Capacity, Nanotechnology, Cathode, Electroanalytical chemistry

1. Introduction

Among various energy storage technologies, rechargeable lithium-ion batteries (LIBs) are considered as an effective and reliable solution to the increasing demand for high-energy density power sources. The high specific energy and power available from LIBs and the prospect to charge and discharge them hundreds of times are the reason for their key importance in electronic portable devices and future development of hybrid vehicles.

When a battery is charged or discharged, the redox reactions change the molecular or crystalline structure of the electrode materials, which often affects their stability, and hence require frequent replacement after several charge-discharge cycles. LIBs weigh less, take less space for a given energy delivery, and offer higher-energy densities than established Ni-Cd and Ni-MH batteries [1]. However, to acquire an established role in the commercial sector, LIBs require improved power density (W/kg), which depends primarily on the performance of the active materials. Li^+ cells operate by a mechanism whereby Li^+ shuttle between two host electrodes, commonly referred to as "insertion electrodes". An insertion compound has two specific properties: the guest ions, Li^+, are mobile between sites in the host network and can be removed from or added to the transition metal oxides host network, thus varying the guest ion concentration [2]. This process is known as intercalation and deintercalation of electrons, occurring at the insertion compound. For transition metal oxides or other chalcogenides, Li^+ occupy sites surrounded by oxygen or chalcogen ions. The sites available are determined by the host structure.

The theoretical capacity, denoted *Q*, of the host material can be calculated from Faraday's first law of electrochemistry, which states that 1 gram equivalent weight of a material will deliver 96,487 C (or 26.8 Ah). For $LiMn_2O_4$, the equivalent weight (*M*) is 180.8 g/mol, having a theoretical capacity of 26.8/180.8=148 mAh g^{-1}.

In LIB, the anode is well optimized and little improvements can be gained in terms of design changes. The cathode, however, shows promise for further enhancements, i.e., improved capacity and stability. Therefore, most research studies are focused on further development of the cathode active materials.

Cathode materials are typically oxides of transition metals, which can undergo oxidation to higher valences when lithium is removed. Among numerous transition metal oxides, $LiMn_2O_4$ has emerged as one of the promising candidates because of its 3D Li^+ diffusion, low cost, abundance, nontoxicity, $Mn^{3+/4+}$ redox couple, and excellent rate capability. $LiMn_2O_4$, however, suffers from low conductivity and capacity fading during cycling. $LiMn_2O_4$ adopts a (3D) structure described as a cubic close packing (ccp) of oxygen atoms with Mn occupying half of the octahedral and Li occupying an eighth of the tetrahedral sites referring to the 16d and 8a sites ($[Li]_{tet}[Mn_2]_{Oct}O_4$), respectively (**Figure 1a**). The $LiMn_2O_4$ morphology corresponds to that of a single crystal with a cubic structure (**Figure 1b**). The scanning confocal electron microscopy (SCEM) image (**Figure 1c**) exhibiting a negative feedback mode verifies the insulating nature of $LiMn_2O_4$. This alternately hinders the diffusion of the mediator to the electrode [3] and contributes to the poor electrochemical performance of the cathode.

http://dx.doi.org/10.5772/62319

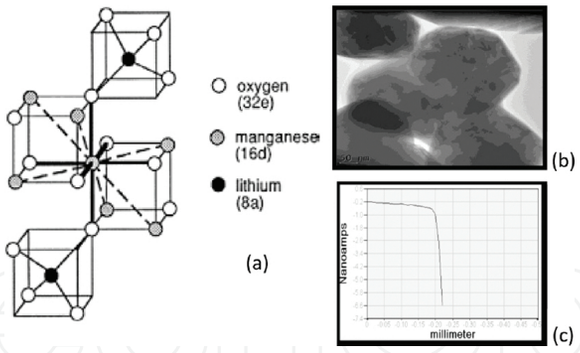

Figure 1. Spinel structure showing the MnO_6 octahedra and Li 8a tetrahedral positions of $LiMn_2O_4$ (a) [4] with its corresponding transmission electron microscopy (TEM; b) and SCEM (c) graphs.

$LiMn_2O_4$ with its poor stability and high rate performance cannot satisfy high-power applications. The reason for this may due to HF generated during cycling when using $LiPF_6$-based electrolyte, which is responsible for the dissolution of manganese. In addition, Mn^{3+} is considered to be the main source of the dissolution of manganese via Hunter's reaction [5]:

$$4H^+ + 2LiMn^{3+}Mn^{4+}O_4 \rightarrow 3(\lambda - MnO_2) + Mn^{2+} + 2Li^+ + 2H_2O$$

The protonated λ-MnO_2 cannot act as a host for Li^+ during cycling because of the strong binding energy of the protons to the oxygen sites around the 16d Mn [6] . This reduces conductance and blocks the transport of electrons or ions, reducing the electrochemical performance of $LiMn_2O_4$.

To solve partially or completely the capacity fading problems, coating the surface of $LiMn_2O_4$ is the easiest functionalization route and offers a suitable approach to avoid the dissolution of Mn^{2+} [7]. Many research studies have confirmed the importance of the structural surface features of cathode materials for their electrochemical performance. It is claimed that, when the surface of cathode materials is coated with oxides and other catalytically active materials, the coatings prevent direct contact with the electrolyte solution, suppress phase transition, improve the structural stability, and decrease the disorder of cations in crystal sites. As a result, side reactions and heat generation during cycling are minimal.

The aim of this study is synthesis and characterization of novel transition metal alloy surface-modified spinel $LiMn_2O_4$ nanocathode materials with high rate discharge capabilities. The coating material consists of Au alloyed with Fe, Pt, and Pd nanoparticles, respectively. The components were selected based on their ability to provide high electronic conductivity where needed and their potential to act as a chemical catalyst for electrochemical reactions at the nanoscale [8]. These alloys are relatively less studied when compared to other transition metal alloys commonly used to form network structures with $LiMn_2O_4$. The modified cathode allows the consumption of smaller amounts of expensive metals, boosting both the catalytic and economic appeals. Moreover, the synergy within the novel composite cathode materials can provide a better connecting network for electron diffusion due to a shortened transportation

path [9] and enhanced phase transition kinetics of Li^+ ion intercalation/deintercalation, which may be ascribed to the nanoscale structure [10]. Emerging applications have therefore steered Li^+ electrode materials in the direction of nanomaterials [11]. The effect of surface functionalization on the conductivity, stability, and high rate performances [12] of $LiMn_2O_4$ was probed by spectroscopic and microscopic techniques along with galvanostatic charge–discharge analyses.

1.1. Significance of nanocatalysis

Nanocatalysis is when nanoparticles are used to catalyze chemical reactions and allow for rapid and selective chemical transformations. Nanomaterials can increase the efficiency of the energy storage and conversion processes as well as device design and performance. The application of bimetallic nanoparticles as catalysts is one of the most active areas of nanoscience [13]. Bimetallic nanoparticles are the combination of two metals in the nanometer range. They can be classified into four types of mixing patterns: core-shell nanoparticles, subcluster nanoparticles, mixed nanoparticles, and multishell nanoparticles [14]. The combination of the two different metals gives rise to an enhancement of specific properties. These properties may be different to those of pure elemental particles and can include unique size-dependent optical, electronic, and catalytic effects [15]. Bimetallic nanocatalysts provide a way to use smaller amounts of an expensive catalyst material, by using a less expensive metal for the core material. For transition metal nanoparticles, the decrease in size to the nanometer length scale increases the surface-to-volume ratio. This, together with the ability to make them in different sizes and shapes, makes them potentially useful in the field of catalysis [16]. It has been proven that the most favorable size for platinum-based electrocatalysis is in the range of 2 to 4 nm [17]. Bimetallic nanoparticles have been proven successful in enhancing the selectivity and rates of many targeted reactions. For example, the hydrogenation rate of simple olefins is increased in the presence of palladium catalysts containing 20% gold when compared to monometallic palladium catalysis [18]. In this study, we investigate how chemically depositing Au-Fe, Au-Pd, and Au-Pt can enhance the conductivity and cyclability of LiMn2O4.

2. Experimental method

Pristine spinel-$LiMn_2O_4$ cathode was prepared following a coprecipitation method [19]. Stoichiometric amounts of LiOH and ($MnAc_2.4H_2O$) with a cationic ratio of Li/Mn=1:2 were dissolved in deionized water and thoroughly mixed. This was followed by evaporation at 100ºC for 10 h. The precursor was further preheated at 400ºC for 1 h and then calcined at 800ºC for 20 h in air to form $LiMn_2O_4$. Subsequently, a multiple-phase emulsion-assisted approach was used to prepare Au-Fe, Au-Pd, and Au-Pt bimetallic nanoparticles with narrow size distributions. This process uses metallic acetates as the metal precursors. For functionalization of $LiMn_2O_4$, the nanoalloy was added to deionized water and allowed to dissolve completely. The crystalline $LiMn_2O_4$ was added to the alloy solution and heated until the solvent evaporates. This was then followed by calcination at 550ºC for 10 h in air. Hereby, the impurities were removed and Mn^{3+} concentration prone to disproportion was reduced and a composite of $Li(M)_xM_{2-x}O_4$ (x=0.02) was constructed.

http://dx.doi.org/10.5772/62319

2.1. Battery assembly

The tested cell consisted of the cathode and a lithium metal anode separated by Celgard microporous membranes to avoid internal short circuit. The electrolyte used was 1 M $LiPF_6$ ethylene carbonate (EC)-dimethyl carbonate (DMC; 1:2, by volume; Ube Chemicals, Japan) solution. All the assembling of the cell was carried out in an argon-filled dry box.

3. Results and discussion

The micrographs of pure and modified $LiMn_2O_4$ samples are shown in **Figure 2**. The pure $LiMn_2O_4$ (a) appear to have primary particles around 50 nm and have the expected spinel shape. The secondary particles of $LiMn_2O_4$ are about 100 nm, which are glomeration congregated tightly by primary particles, indicating that the crystals of the spinel $LiMn_2O_4$ grow well and have interparticle boundaries. The micrograph of $LiFeAu_{0.02}Mn_{1.98}O_4$ (b) shows two types of particles with different particle sizes. The larger particles are that of the pristine sample, exemplified by an octahedral shape. The FeAu nanoparticle surface feature corresponds to cubic- or hexagonal-shaped particles of about 20 nm, which are heterogeneously dispersed across the pristine $LiMn_2O_4$ particles. $LiPdAu_{0.02}Mn_{1.98}O_4$ (c) shows well-dispersed PdAu nanoparticles. The $LiPdAu_{0.02}Mn_{1.98}O_4$ nanoparticles retained a well-developed octahedral structure with sharp edges after surface treatment and exhibited particle sizes in the range of 20–50 nm. The micrograph of $LiPtAu_{0.02}Mn_{1.98}O_4$ (d) shows smoother particles. The surface of $LiPtAu_{0.02}Mn_{1.98}O_4$ appears infused with the PtAu nanoparticles having a bumpy morphology with only some aggregates [20]. All the coated $LiMn_2O_4$ samples have increased surface area, which favors the penetration of electrolyte, decreasing the diffusion length of Li^+ and electrons, and improves the overall activity of the cathode.

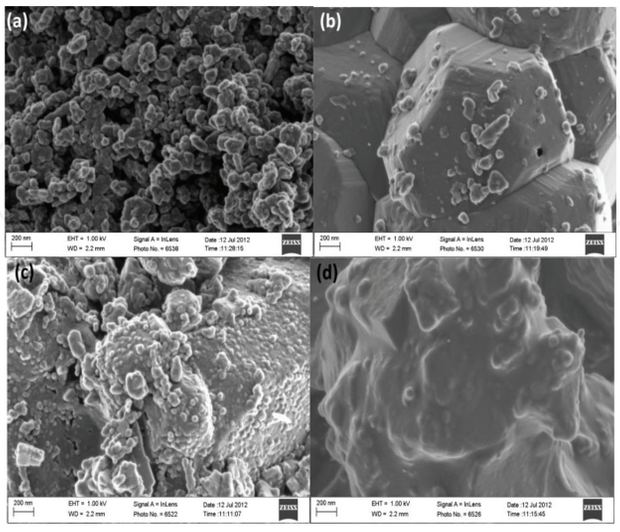

Figure 2. SEM micrographs of $LiMn_2O_4$ (a), $LiFeAu_{0.02}Mn_{1.98}O_4$ (b), $LiPdAu_{0.02}Mn_{1.98}O_4$ (c), and $LiPtAu_{0.02}Mn_{1.98}O_4$ (d) calcined at 880°C.

Atomic force microscopy (AFM) was used to characterize samples at the microscope level, with accurate resolution ranging from 100 to <1 μm. **Figure 3** shows the AFM surface morphology images of $LiMn_2O_4$ and $Li(M)_{0.02}Mn_{1.98}O_4$ particles. Compared to scanning electron microscopy (SEM), AFM provides extraordinary topographic contrast direct height measurements and unobstructed views of surface features. The darker regions are indicative of the partial heterogeneous surface coverage. The $LiMn_2O_4$ (a) image reveals clear globular features. It is evident that this surface yields a large degree of surface roughness. The size distribution was broad and the maximum shifted towards an average diameter of 60 nm. It has been known that the particle size influences directly on battery performance; hence, materials generally employed for battery application are >1 μm. To apprehend the high rate capabilities of the cathode, it is necessary to employ active materials with particles in the nanometer range.

The $LiFeAu_{0.02}Mn_{1.98}O_4$ (b) sample yields uniform surface roughness. This feature may be attributed to the FeAu coating layer, which attributed to compact surface architecture. Evidently, the particle size distribution has narrowed down and the maximum has shifted towards an average diameter of 40 nm. Based on prior research [21], it is clear that the smaller the crystallite size, the bigger the specific surface area, hence permitting favourable conditions for improved cycling performance. $LiPdAu_{0.02}Mn_{1.98}O_4$ (c) revealed uniform surface roughness, and the particle sizes distribution is narrow with an average maximum diameter of 30 nm. A new phase possessed by $LiPtAu_{0.02}Mn_{1.98}O_4$ is evident in (d). The observed changes could be the result of the film volume increase, which is due to the uptake of PtAu onto the $LiMn_2O_4$ matrix [22]. AFM characterization confirmed that the PtAu alloy is well adherent to the surface. This agrees with the SEM image showing PtAu particle infusion. The surface feature may be beneficial for more rapid Li^+ transportation facilitating better high rate performances, including low polarization and better structural stability.

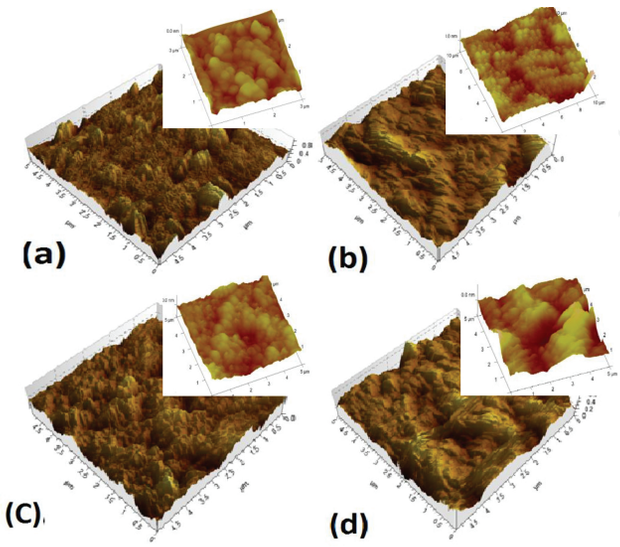

Figure 3. AFM images of $LiMn_2O_4$ (a), $LiFeAu_{0.02}Mn_{1.98}O_4$ (b), $LiPdAu_{0.02}Mn_{1.98}O_4$ (c), and $LiPtAu_{0.02}Mn_{1.98}O_4$ (d).

http://dx.doi.org/10.5772/62319

Figure 4 shows the X-ray diffraction (XRD) peaks of $LiMn_2O_4$ and $Li(M)_{0.02}Mn_{1.98}O_4$ cathode materials. All the peaks correspond to a single phase of cubic spinel structure with a space group *Fd3m* in which the Li^+ occupy the tetrahedral (8a) site and manganese and the substituted metal occupy the octahedral (16d) site. All the peaks were indexed as the spinel phase (JCPDS: 35-0782). These results indicate that $LiMn_2O_4$ retains its spinel structure after modification and the addition of the bimetalic alloys in the preparation process does not alter the phase purity of the product. The main diffraction peaks of cubic spinel $LiMn_2O_4$ phase, such as (111), (311), and (400), is well developed. No additional peak was observed for $Li(M)_{0.02}Mn_{1.98}O_4$; however, the lattice constants change slightly compared to pristine spinel powder from 8.2609 to 8.2600 Å. The ionic radius of Mn^{4+} is smaller than that of Mn^{3+}. Therefore, the decrease of lattice constant is indicative of an increase in Mn^{4+} ion concentration in the spinel [23]. The smaller MnO_6 octahedra suggest a stable MnO_6 framework and lower activation energy, which supports high rate electrochemical cycling [24]. Concomitantly, the coated samples with almost the same structure as $LiMn_2O_4$ support easy Li^+ diffusion during the charge-discharge process. This finding was validated by both solid-state nuclear magnetic resonance (NMR) magic angle spinning (MAS) and cycliability studies.

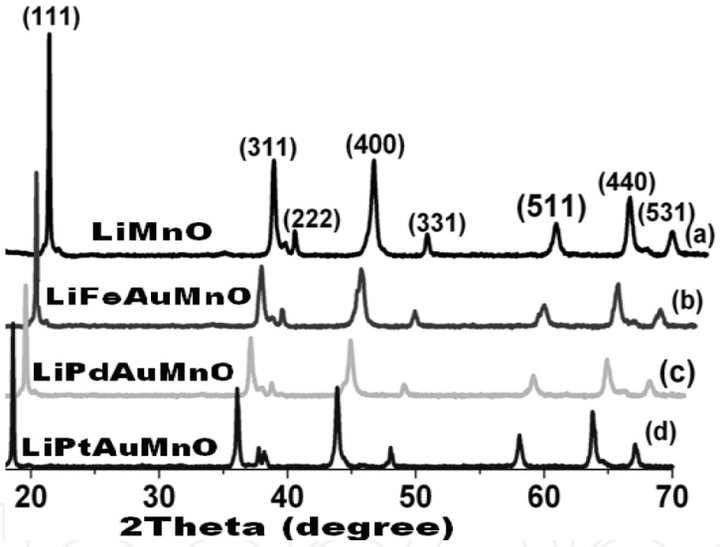

Figure 4. XRD spectra of $LiMn_2O_4$ and $Li(M)_{0.02}Mn_{1.98}O_4$ cathode materials.

Complementary to XRD, NMR is a useful tool to obtain information on the chemical and structural local environment of the nucleus under observation (^7Li). Any relevant structural change will affect the NMR spectrum, such as the change in bonding geometry, bonding distance, or nuclear charge [25]. The NMR spectra of $LiMn_2O_4$ and $Li(M)_{0.02}Mn_{1.98}O_4$ cathode materials are shown in **Figure 5**. At 16 kHz spinning speed, a high-resolution MAS NMR spectrum was obtained. The ^7Li-NMR spectrum of $LiMn_2O_4$ shows that there are two different types of lithium sites. The main peak at about 530 ppm is assigned to Li^+ in the tetrahedral 8a site of the spinel structure; the small resonances at about 580 and 615 ppm ($Li(M)_{0.02}Mn_{1.98}O_4$) are ascribed to Li^+ residing near the higher oxidation state manganese ions (Mn^{4+}) [26]. The lithium moves onto the tetrahedral site due to M_x atom propensity for the octahedral sites.

Therefore, the isotropic resonance at 511 ppm for $LiMn_2O_4$ is assigned to Li^+ ions in the tetrahedral 8a site, whereas the isotropic resonances at ~680 and 835 ppm for $Li(M)_{0.02}Mn_{1.98}O_4$ samples are assigned to lithium present in the proximity of higher oxidation state manganese ions (Mn^{4+}). These results suggest that the samples are pure and structural integrity is maintained.

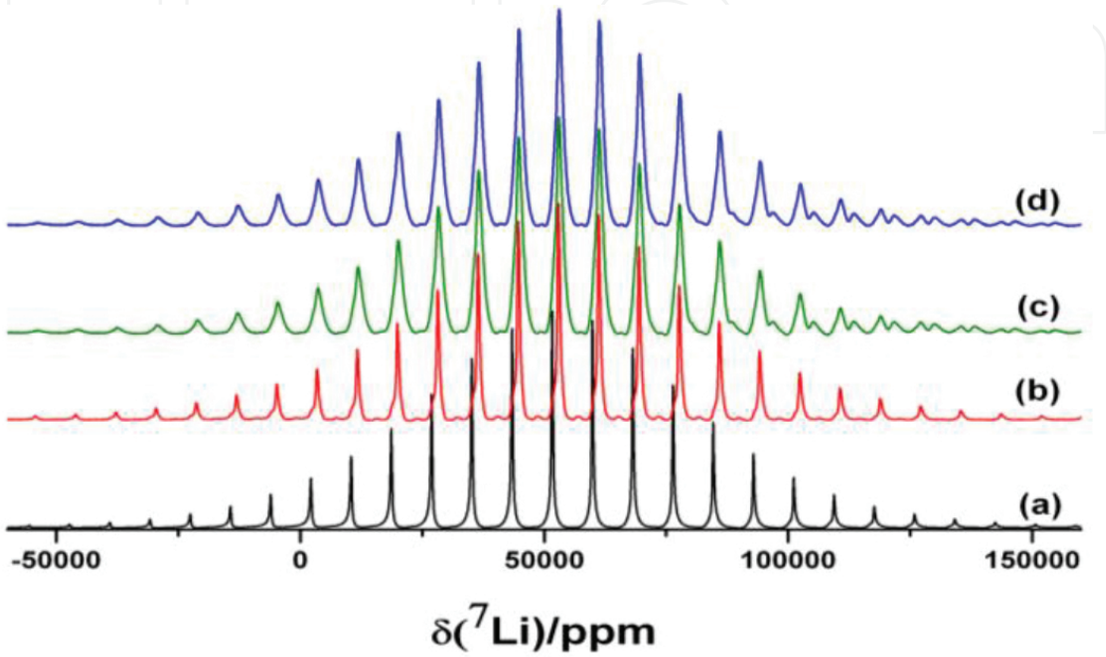

Figure 5. ^7Li NMR spectra of $LiMn_2O_4$ (a) and $Li(M)_{0.02}Mn_{1.98}O_4$ (b–d) at 16 kHz.

3.1. Electrochemical analysis

The ability of the metal alloy to enhance $LiMn_2O_4$ redox properties has been confirmed. The galvanostatic curve of $LiMn_2O_4$ (**Figure 6a**) is compared to that of $Li(M)_{0.02}Mn_{1.98}O_4$ cathodes (**Figure 6b–d**) at 0.1 mV s^{-1}. The pristine $LiMn_2O_4$ shows several peaks, which are ascribed to the $Mn^{3+/4+}$ redox reaction and constituents in the cathode material. Similar peak pairs are also found in the profiles of all functionalized samples with some shifts in potential and current. This demonstrates that coating does not change the electrochemical behavior but only the kinetics of $LiMn_2O_4$. The pair of peaks observed at ~3.2 V in the profiles of $Li(M)_{0.02}Mn_{1.98}O_4$ is well defined at 0.1 mV s^{-1}. This peak pair has been considered as the signature of $M^{3+/4+}$ redox reactions or its partial influence to a lesser extent in alloy functionalized spinel cathode material. Therefore, peak A2 is less pronounced in the pristine $LiMn_2O_4$ curve. $Li(M)_{0.02}Mn_{1.98}O_4$ has reduced anodic/cathodic potential differences compared to $LiMn_2O_4$, which is suggestive of smaller polarization due to the faster insertion/extraction of Li^+ ions in the spinel structure. This indicates that effective electron hopping between Mn^{3+} and Mn^{4+} lowers the potential barrier for Li^+ diffusion within the spinel lattice [27]. The faster lithium mobility enhances high rate performances [28]. This was corroborated by the high rate cycliability study.

http://dx.doi.org/10.5772/62319

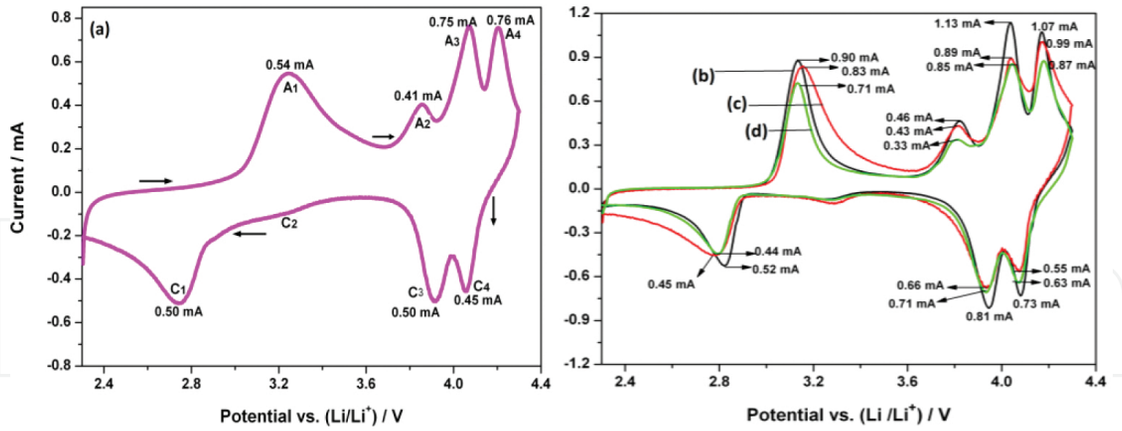

Figure 6. Cyclic voltammograms of $LiMn_2O_4$ (a), $LiFeAu_{0.02}Mn_{1.98}O_4$ (b), $LiPdAu_{0.02}Mn_{1.98}O_4$ (c), and $LiPtAu_{0.02}Mn_{1.98}O_4$ (d) cycled at 0.1 mV s^{-1}.

Figure 7 shows the cycling performance of $LiMn_2O_4$ and $Li(M)_{0.02}Mn_{1.98}O_4$ [M=FeAu (green), PdAu (black), and PtAu (red)] at 0.1 and 10 C discharge current rates. All the coated samples have stable discharge capacities at 10 C but show gradual decrease in capacity at 0.1 C. At 10 C, the discharge capacity decreases early for $LiFeAu_{0.02}Mn_{1.98}O_4$, with only 54% capacity retention. This suggests that ferric ions are probably involved in the reduction process leading to Fe^{2+}. When the cycling potential range is enlarged to overcome electrode kinetic limitations, the $Li(M)_{0.02}Mn_{1.98}O_4$ samples delivered relevant discharge capacities (70, 80, and 90 mAh g^{-1}) at high current density compared to that of $LiMn_2O_4$ (45 mAh g^{-1}). The $LiPtAu_{0.02}Mn_{1.98}O_4$ material exhibits the best capacity retention at 10 C with 88.7 mAh g^{-1} at the 50th cycle (99% capacity retention).

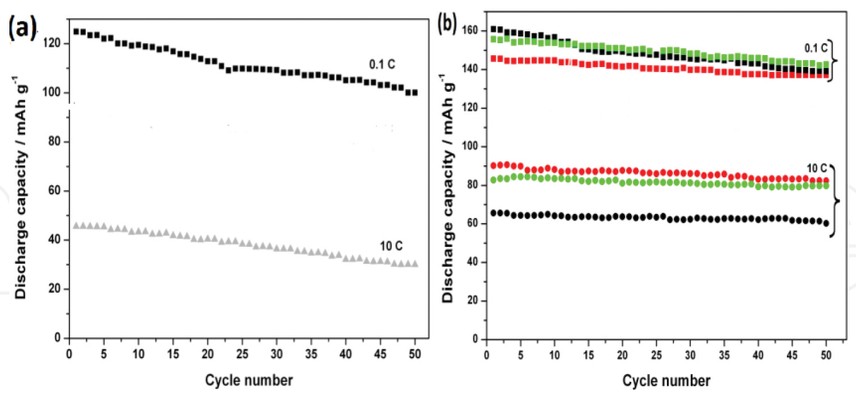

Figure 7. Cyclability of (a) $LiMn_2O_4$ and (b) $LiFeAu_{0.02}Mn_{1.98}O_4$ (green), $LiPdAu_{0.02}Mn_{1.98}O_4$ (black), and $LiPtAu_{0.02}Mn_{1.98}O_4$ (red) at 0.1 and 10 C.

The coulombic energy efficiency, which is the fraction of the electrical charge stored during charging that is recoverable during the discharge [29] of $LiMn_2O_4$, $LiFeAu_{0.02}Mn_{1.98}O_4$, $LiPdAu_{0.02}Mn_{1.98}O_4$, and $LiPtAu_{0.02}Mn_{1.98}O_4$ at 0.1 and 10 C discharge current rates, was computed using Equation (1):

$$CE = \frac{\int_0^t I_d dt}{\int_0^t I_c dt} \quad (1)$$

where I_d is the discharging current and I_c is the charging current, which are constant in most operations. With the increase in current density, the efficiency decreased to some extent. However, even at a current of 10 C, a maximum efficiency of 99% was obtained, confirming the excellent performance of the $Li(M)_{0.02}Mn_{1.98}O_4$ modified cathodes. The losses that reduce coulombic efficiency are primarily due to the loss in charge due to secondary reaction, such as the electrolysis of water or other redox reactions in the battery. The fading rate of $LiMn_2O_4$ at 0.1 C was reduced by ~15% by surface modification. At higher C rate, however, the fading rate was less apparent. The improved cycling performance is attributed to the stabilization of the spinel structure by metal cations [30]. An electrochemical impedance study [31] further corroborated the excellent high rate performance of the modified cathode. **Figure 8** shows that the total impedance observed for $Li(M)_{0.02}Mn_{1.98}O_4$ was moderately lower than that of $LiMn_2O_4$. The values obtained fitting to an equivalent circuit are shown in **Table 1**, confirming the integration of a conductive surface material.

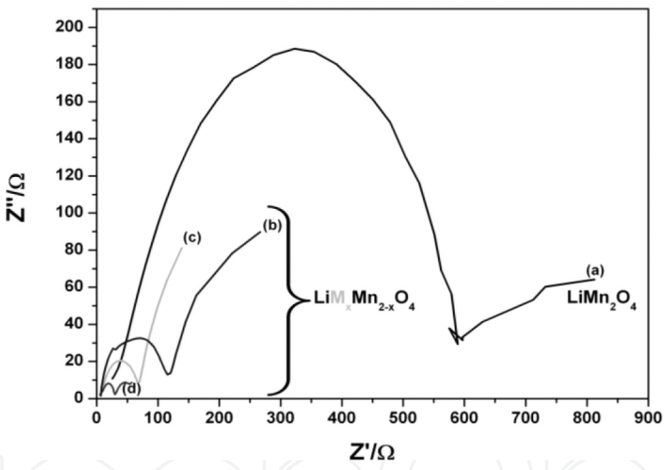

Figure 8. Nyquist plot of (a) $LiMn_2O_4$ and $Li(M)_{0.02}Mn_{1.98}O_4$ (b–d).

	$LiMn_2O_4$(a)	$LiFeAu_xMn_{2-x}O_4$(b)	$LiPdAu_xMn_{2-x}O_4$(c)	$LiPtAu_xMn_{2-x}O_4$(d)
R_{ct} (Ω)	140	93.25	80.86	30.85
f_Φ (kHz)	0.93	4.47	5.75	6.47

Table 1. Electrochemical impedance spectroscopy (EIS) characterization data of $LiMn_2O_4$ and alloy functionalized cathodes.

The kinetic index (calculated from f_Φ), explained by the time constant (τ), where τ is inversely proportional to the frequency and solution resistance as expressed by Equation (2), was faster

http://dx.doi.org/10.5772/62319

at the modified electrodes (2.41×10^{-4} s rad^{-1}) compared to the pure material (3.41×10^{-4} s rad^{-1}). This confirmed both the conductive and catalytic influences of the nanoalloy [32].

$$\tau = \frac{1}{4\pi f_{\phi}} \sqrt{1 + \frac{R}{R_s}} \tag{2}$$

Moreover, all $Li(M)_{0.02}Mn_{1.98}O_4$ samples showed improved discharge current densities. These samples exhibited two plateaus in the discharge curves, due to the two-step reduction and oxidation process, which is a characteristic of lithium manganese oxide spinel [33]. This further supports the XRD finding showing that the spinel structure of $LiMn_2O_4$ is retained after surface modification. The initial discharge capacities of $Li(M)_{0.02}Mn_{1.98}O_4$ increase due to the decrease in Mn^{3+} content. This means that the spinel phase is stabilized by the surface modification, and the alloy does not block the lithium pathway. Instead, the larger interface area provides more Li^+ ions for diffusion; therefore, the specific capacity is increased [34,35].

4. Conclusion

A novel transition metal alloy (FeAu, PdAu, and PtAu), functionalized $LiMn_2O_4$, was successfully synthesized. Excellent reproducibility was obtained when electrodes were cycled at high discharge rates. The $Li(M)_{0.02}Mn_{1.98}O_4$ cathode materials were lattice defective and phase pure and exhibited improved rate capabilities and improved electrochemistry compared to the pristine $LiMn_2O_4$. These improvements were attributed to enhanced electronic conductivity, lithium diffusivity due to the reduction in particle size, and structural stability. Microscopic results revealed that the composite cathode materials had well-crystallized particles and more regular morphological structures with narrow size distributions, which effectively accommodated the structural transformations that occur during Li^+ insertion. Moreover, these materials showed to be uniquely durable and might be used extremely efficient, making it economically viable. The enhancement of the capacity retention and higher electrode coulombic efficiency of the modified materials were significant, especially at high C rate.

Author details

Natasha Ross* and Emmanuel I. Iwuoha

*Address all correspondence to: nross@uwc.ac.za

SensorLab, Department of Chemistry, University of Western Cape, Private Bag X17, Bellville , Cape Town, South Africa

References

[1] Lu K. Materials in Energy Conversion, Harvesting, and Storage (111888910X); 2014. ISBN: 978-1-118-88910-7. 448.

[2] Eriksson T. $LiMn_2O_4$ as a Li-Ion Battery Cathode; From Bulk to Electrolyte Interface. Eklunds hofs Grafiska AB, Uppsala; 2001. Available at: https://uu.diva-portal.org/smash/get/diva2:160906.

[3] Guo YG, Hu JS, Wan LJ. Nanostructured materials for electrochemical energy conversion and storage devices. Adv. Mater. 2008;20:2878.

[4] Hunter JC. Preparation of a new crystal form of manganese dioxide: λ-MnO_2. J. Solid State Chem. 1981;39:142.

[5] Pasquier BA, Courjal AD, Larcher P, Amatucci D, Gerand G. Mechanism for limited 55°C storage performance of $Li_{1.05}Mn_{1.95}O_4$ electrodes. J. Electrochem Soc. 1999;146:428.

[6] Ohzuku T, Makimura Y. Layered lithium insertion material of $LiCo_{1/3}Ni_{1/3}Mn_{1/3}O_2$ for lithium-ion batteries. Chem. Lett. 2001;30:642.

[7] Mui SC, Trapa PE, Huang B, Soo PP, Lozow MI, Wang TC, Cohen RE, Mansour AN, Mukerjee S, Mayes AM, Sadoway DR. Block copolymer-templated nanocomposite electrodes for rechargeable lithium batteries. J. Electrochem. Soc. 2002;149:A1610.

[8] Spong AD, Vitins G, Owen JR. A solution-precursor synthesis of carbon-coated $LiFePO_4$ for Li-ion cells. J. Electrochem. Soc. 2005;152:A2376.

[9] Arico AS, Scrosati B, Tarascon JM, Van Schalkwijk W. Nanostructured materials for advanced energy conversion and storage devices. Nat. Mater. 2005;4:366.

[10] Xiong H, Guo J, Amemiya S. Probing heterogeneous electron transfer at an unbiased conductor by scanning electrochemical microscopy in the feedback mode. Anal. Chem. 2007;79:2735–2744.

[11] Haruta M. When gold is not noble: catalysis by nanoparticles. Chem. Rec. 2003;3:75.

[12] Liu J, Manthiram A. Materials challenges and opportunities of lithium ion batteries. Chem. Mater. 2009;21:1695.

[13] Jellinek J. Nanoalloys: from theory to application. Faraday Discuss. 2008;138:1.

[14] Liang AS, Caruso F. Gold nanoparticle-based core-shell and hallow spheres and ordered assemblies thereof. Chem. Mater. 2003;15:3176.

[15] Ferrando JR, Johnston RL. Nanoalloys: from theory to applications of alloy clusters and nanoparticles. Chem. Rev. 2008;108:845.

[16] Burda C, Narayanan R, El-Sayed MA. Chemistry and properties of nanocrystals of different shapes. Chem. Rev. 2005;105:1025.

[17] Zhao D, Xu B-Q. Enhancement of Pt utilization in electrocatalysts by using gold nanoparticles. Angew. Chem. 2006;30:5077.

[18] Shah A, Rahman L-u, Qureshi R, Rehman Z-u. Synthesis, characterization and applications of bimetallic (Au-Ag, Au-Pt, Au-Ru) alloy nanoparticles. Rev. Adv. Mater. Sci. 2012;30:133.

[19] Liu Q, Wang S, Tan H, Yang Z, Zeng J. Preparation and doping mode of doped $LiMn_2O_4$ for Li-ion batteries. Energies 2013;6:1718.

[20] Li X, Xu Y, Wang C. Novel approach to preparation of $LiMn_2O_4$ core/$LiNiXMn_{2-x}O_4$ shell composite. Appl. Surf. Sci. 2009;255:5651.

[21] Matsuda K, Taniguchi I, Ronbunshu KK. Particle properties of $LiMn_2O_4$ fabricated by ultrasonic spray. Pyrolysis method. J. Power Sources 2003;29:232.

[22] Otero F, Rodriguez J. Reinterpretation of polypyrrole electrochemistry after consideration of conformational relaxation processes. J. Phys. Chem. B 1997;101:3688.

[23] Hunter JC. Preparation of a new crystal form of manganese dioxide. J. Solid State Chem. 1981;39:142.

[24] Zhang D, Popov BN, White RE. Electrochemical investigation of $CrO_{2.65}$ doped $LiMn_2O_4$ as a cathode material for lithium-ion batteries. J. Power Sources 1998;76:81.

[25] Lee YJ, Grey CP. ^{6}Li magic-angle spinning (MAS) NMR study of electron correlations, magnetic ordering, and stability of lithium manganese (III) oxides. Chem. Mater. 2000;12:3871.

[26] Kumar VG, Gnanaraj JS, Ben-David S, Pickup DM, Van-Eck ERH, Gedanken A, Aurbach D. An aqueous reduction method to synthesize spinel-$LiMn_2O_4$ nanoparticles as a cathode material for rechargeable lithium-ion batteries. Chem. Mater. 2003;15:4211.

[27] Zhang X, Zheng H, Battaglia V, Axelbaum RL. Electrochemical performance of spinel $LiMn_2O_4$ cathode materials made by flame-assisted spray technology. J. Power Sources 2011;196:3640.

[28] Atanasov M, Barras J-L, Benco L, Daul C. Theoretical studies on the electronic properties and the chemical bonding of transition metal complexes using DFT and ligand field theory. J. Am. Chem. Soc. 2000;122:4718.

[29] Braun PV, Cho J, Pikul JH, King WP, Zhang H. High power rechargeable batteries. Curr. Opin. Solid State Matter 2012;16:186–198.

[30] Tang D, Ben L, Sun Y, Chen B, Yang Z, Gu L, Huang X. Electrochemical behavior and surface structural change of $LiMn_2O_4$ charged to 5.1 V. J. Mater. Chem. A 2014;2:14519–14527.

[31] Chen J. Recent progress in advanced materials for lithium ion batteries. Materials 2013;6:156–183.

[32] Mendelson MI. Learning Bio-Micro-Nanotechnology. CRC Press; 2012.

[33] Thirunakaran R, Gopukumar S, Rajalakshmi R. Cerium and zinc: dual-doped $LiMn_2O_4$ spinels as cathode material for use in lithium rechargeable batteries. J. Power Sources 2009;187:565.

[34] Wang X, Tanaike O, Kodama M, Hatori H. High rate capability of the Mg-doped Li-Mn-O spinel prepared via coprecipitated precursor. J. Power Sources 2007;168:282–287.

[35] Guohua Li, Ikuta H, Uchida T, Wakihara M. The spinel phases $LiM_yMn_{2-y}O_4$ (M=Co, Cr, Ni) as the cathode for rechargeable lithium batteries. J. Electrochem. Soc. 1996;143:178–182.